

Bayesian extraction of TMC-free collectivity in p+p and p+Pb collisions at the LHC

Shuang Guo,^{1,2} Jia-Lin Pei,^{1,2,*} Guo-Liang Ma,^{1,2,†} and Adam Bzdak^{3,‡}

¹Key Laboratory of Nuclear Physics and Ion-beam Application (MOE),
Institute of Modern Physics, Fudan University, Shanghai 200433, China

²Shanghai Research Center for Theoretical Nuclear Physics,
NSFC and Fudan University, Shanghai 200438, China

³AGH University of Krakow,
Faculty of Physics and Applied Computer Science, 30-059 Kraków, Poland

A central challenge in understanding the origin of collective flow-like signatures in small collision systems calls for a reliable method to disentangle genuine collective flow from substantial background correlations, especially those arising from transverse momentum conservation (TMC). A Bayesian inference framework is developed to integrate TMC calculations with the LHC-ATLAS data on long-range multiparticle azimuthal correlation observables, thereby extracting genuine collective flow in small systems. Our analysis indicates that while the genuine elliptic and triangular flow (v_2 and v_3) are similar, the $p+p$ and $p+Pb$ systems exhibit distinct TMC backgrounds, TMC-flow interplay, and v_2 - v_3 correlations. We demonstrate that the genuine v_2 and v_3 are well described by the measured four-particle $v_2\{4\}$ and two-particle $v_3\{2\}$ in $p+Pb$ collisions, whereas these measurements systematically underestimate the genuine flow in $p+p$ collisions, due to competing contributions from TMC effects. This establishes a robust and data-driven approach, providing renewed theoretical insight into collective behavior free from TMC contamination in small collision systems.

I. INTRODUCTION

Quark-gluon plasma (QGP), a deconfined state of matter where quarks and gluons are liberated from confinement, forms in the extreme, hot and dense environment created by high-energy nucleus-nucleus collisions at the Relativistic Heavy Ion Collider (RHIC) and the Large Hadron Collider (LHC) [1–7]. The experimental results have shown that this new type of nearly perfect fluid can translate initial spatial geometry or initial energy density fluctuations into momentum anisotropy of the final particles through the pressure gradient in hydrodynamics [8–17], resulting in the emergence of a strong collective flow in A+A collisions [18, 19]. To quantify azimuthal anisotropy in the transverse momentum plane, the particle distribution is parameterized by a Fourier series $\frac{dN}{d\varphi} \propto 1 + \sum_n v_n \cos[n(\varphi - \Psi_n)]$. This expansion defines the anisotropic flow coefficients, where v_1 , v_2 , v_3 , and v_4 correspond to directed, elliptic, triangular, and quadrangular flow, respectively [20–22]. Experimentally, flow coefficients are extracted using various methods, including the event plane method [23, 24], two-particle correlations [25, 26], and multi-particle cumulants $v_n\{k\}$. The latter is particularly valued for its ability to suppress non-flow effects [27, 28]. These non-flow correlations, which contaminate the flow signal, originate from various sources: short-range ones such as jets, resonance decays, and Bose-Einstein correlations, as well as long-range ones like those induced by transverse momentum conservation (TMC) [29–32].

Over the past decade, collective flow measurements have been performed in a variety of colliding systems, including $p+p$ and $p+Pb$ collisions at the LHC [33–38], as well as $p+Au$, $d+Au$, and ^3He+Au collisions at RHIC [39–43]. Surprisingly, the ridge structure, characterized by a small azimuthal separation and an extended longitudinal correlation, which is regarded as direct evidence for collective flow in A+A collisions [44, 45], has also been observed in small systems such as $p+p$ and $p+A$. This finding raises the question of whether QGP could also be produced in such small colliding systems. Numerous theoretical efforts have been made to explain the emergence of collective flow in small colliding systems. The proposed explanations can be broadly categorized into several mechanisms. Firstly, similar to the scenario in large systems, hydrodynamic models describe how the pressure gradient of a possible QGP droplet in small systems converts initial geometric asymmetries into final-state momentum anisotropy [46–50]. Alternatively, transport models attribute flow signals to a parton escape mechanism, where the anisotropic escape probability of partons generates the observed v_n [51–56]. Lastly, the color glass condensate (CGC) framework offers an initial-state mechanism to explain two-particle long-range correlations and the Fourier v_n coefficients. In this framework, such

*jlpei22@m.fudan.edu.cn

†glma@fudan.edu.cn

‡bzdak@fis.agh.edu.pl

correlations can be generated through the emission of two gluons in the glasma Feynman diagrams [57–63].

Conservation laws represent another significant source of azimuthal correlations among particles [64–67], among which transverse momentum conservation (TMC) plays a crucial role in explaining collective flow behavior in small colliding systems. We have found that the TMC effect induces positive $2k$ -particle elliptic flow cumulants $c_2\{2k\}$, which scale as $1/(N-2k)^{2k}$ [68], where N is the number of particles constrained by transverse momentum conservation. Furthermore, when TMC interacts with hydrodynamics-like elliptic flow, the four-particle cumulant $c_2\{4\}$ undergoes a sign change. This behavior provides a natural explanation for the observed multiplicity-dependent sign change of $c_2\{4\}$, $c_3\{2\}$ and $c_3\{4\}$ in small systems at the LHC [69, 70]. Our recent calculations of the four-particle symmetric cumulants $sc_{2,3}\{4\}$ and $sc_{2,4}\{4\}$ show that the observed correlations originate from TMC at low multiplicities, with collective flow becoming increasingly dominant as the particle number N rises, which aligns well with ATLAS measurements [71, 72].

Since the TMC theoretical framework has demonstrated good agreement with experimental observations in small collision systems, it is natural to explore whether collective flow signals can be quantitatively extracted from experimental data within this approach. Our goal is to identify a set of collective flow parameters that can simultaneously describe multiple experimental observables in small systems. In previous studies, calculations of multi-particle correlators $c_n\{k\}$ that include both TMC and flow effects typically rely on manually fixing key parameters, such as the elliptic and triangular flow coefficients v_2 and v_3 , as well as the transverse momentum of the correlated particles and the event-averaged $\langle p^2 \rangle$. While this tuning strategy can reproduce individual observables, different parameter choices are often required for different measurements, limiting the predictive power of the approach and preventing a systematic estimation of parameter uncertainties.

A more robust and principled approach to extract these parameters directly from experimental data is offered by Bayesian inference [73]. This statistical framework provides a powerful tool for inverse problems, allowing for the simultaneous determination of multiple parameters and a rigorous assessment of their uncertainties. Within heavy-ion physics, Bayesian methods have already been successfully employed for the precise extraction of fundamental properties, such as the specific shear viscosity [74–81], nuclear structure [82, 83], the equation of state (EoS) of nuclear matter [84–88], and jet quenching properties [89], demonstrating their capability to constrain theoretical models with complex dependencies. Therefore, in this work, we will simultaneously constrain the collective flow parameters v_2 and v_3 in $p+p$ and $p+Pb$ collision systems using four experimental observables $c_2\{4\}$, $c_3\{2\}$, $c_3\{4\}$, and $sc_{2,3}\{4\}$ from the ATLAS experiment [90–92]. We further incorporate the dependence of collective flow on charged-particle multiplicity N_{ch} by parameterizing its functional form. This approach not only enables the unified extraction of collective flow properties from experimental measurements, but also facilitates the investigation of pure and genuine collective flow in small collision systems, free from TMC-induced contributions.

This paper is structured as follows. Section II outlines the calculation of cumulants, including $c_2\{4\}$, $c_3\{2\}$, $c_3\{4\}$, and the four-particle symmetric cumulant $sc_{2,3}\{4\}$, based on transverse momentum conservation and flow effects. Section III introduces Bayes’ theorem and elaborates on the specific Bayesian inference procedure employed in this work. In Sec. IV, we present results obtained under two distinct parameter settings, which provide an excellent description of the experimental data. In particular, the inferred collective flow coefficients v_2 and v_3 are compared with the ATLAS measurements of multi-particle azimuthal correlations using the sub-event cumulant method. We further provide a detailed discussion of the collective flow behavior in the two small collision systems, together with a comparative analysis of the different physical contributions in $p+p$ and $p+Pb$ collisions. Finally, Sec. V summarizes our findings and highlights their potential implications for investigating collective flow in small collision systems, with an emphasis on suppressing non-flow backgrounds.

II. CUMULANT AND SYMMETRIC CUMULANT FROM TMC AND FLOW

We begin by outlining the theoretical framework for transverse momentum conservation (TMC), which serves as a baseline source of correlations among final-state particles. In an N -particle system with imposed transverse momentum conservation, i.e., $\vec{p}_1 + \dots + \vec{p}_N = 0$, the k -particle ($k < N$) transverse momentum probability distribution $f_k(\vec{p}_1, \dots, \vec{p}_k)$ is given by [67–69]:

$$f_k(\vec{p}_1, \dots, \vec{p}_k) = f(\vec{p}_1) \cdots f(\vec{p}_k) \frac{N}{N-k} \times \exp\left(-\frac{(p_{1,x} + \dots + p_{k,x})^2}{2(N-k)\langle p_x^2 \rangle_F} - \frac{(p_{1,y} + \dots + p_{k,y})^2}{2(N-k)\langle p_y^2 \rangle_F}\right), \quad (1)$$

where $f(\vec{p})$ denotes the single-particle distribution function, with only v_2 and v_3 effects considered in our calculations,

$$f(\vec{p}) = \frac{g(p)}{2\pi} (1 + 2v_2(p) \cos[2(\phi - \Psi_2)] + 2v_3(p) \cos[3(\phi - \Psi_3)]), \quad (2)$$

$$p_x = p \cos(\phi), \quad p_y = p \sin(\phi), \quad (3)$$

$$\langle p_x^2 \rangle_F = \frac{1}{2} \langle p^2 \rangle_F (1 + v_{2F}), \quad \langle p_y^2 \rangle_F = \frac{1}{2} \langle p^2 \rangle_F (1 - v_{2F}), \quad (4)$$

$$\langle p^2 \rangle_F = \frac{\int_F p^2 f(\vec{p}) d^2 \vec{p}}{\int_F f(\vec{p}) d^2 \vec{p}}, \quad (5)$$

$$v_{2F} = \frac{\int_F v_2(p) g(p) \cos(2\Psi_2) p^2 d^2 p}{\int_F g(p) p^2 d^2 p}, \quad (6)$$

and F denotes the full phase space.

We compute the following cumulants within this framework: the four-particle elliptic cumulant $c_2\{4\}$, the two- and four-particle triangular cumulants $c_3\{2\}$ and $c_3\{4\}$, and the four-particle symmetric cumulant $sc_{2,3}\{4\}$.

For example,

$$c_2\{4\} = \left\langle e^{i2(\phi_1 + \phi_2 - \phi_3 - \phi_4)} \right\rangle - 2 \left\langle e^{i2(\phi_1 - \phi_2)} \right\rangle^2. \quad (7)$$

The detailed procedures for calculating the cumulants are summarized as follows:

$$\begin{aligned} \left\langle e^{i2(\phi_1 - \phi_2)} \right\rangle_{p_1, p_2} &= \frac{\int_0^{2\pi} e^{i2(\phi_1 - \phi_2)} f_2(\vec{p}_1, \vec{p}_2) d\phi_1 d\phi_2}{\int_0^{2\pi} f_2(\vec{p}_1, \vec{p}_2) d\phi_1 d\phi_2} \\ &\approx A_0 + A_1 Y_A + \frac{1}{2} A_2 Y_A^2, \end{aligned} \quad (8)$$

where the form of $f_2(\vec{p}_1, \vec{p}_2)$ is taken from Eq. (1). Assuming $p_1 = p_2 = p$, we obtain:

$$Y_A = -\frac{p^2}{(N-2) \langle p^2 \rangle_F}, \quad (9)$$

and

$$\begin{aligned} A_0 &= v_2^2, \\ A_1 &= 2v_2^2 + v_3^2 - v_2 v_{2F} \cos(2\Psi_2), \\ A_2 &= 1 + 6v_2^2 + \frac{v_{2F}^2}{2} + 3v_2^2 v_{2F}^2 + 4v_3^2 + 2v_{2F}^2 v_3^2 - 8v_2 v_{2F} \cos(2\Psi_2) + \frac{1}{2} v_2^2 v_{2F}^2 \cos(4\Psi_2). \end{aligned} \quad (10)$$

The results in Eq. (10) stem from expanding the exponential term in Eq. (1). As for the numerator in Eq. (8), we expand it to the second order, i.e., $\exp(-X) \approx 1 - X + \frac{X^2}{2}$, since the first non-vanishing pure TMC term, the first term of A_2 in Eq. (10), appears at $\frac{X^2}{2}$. However, for the denominator in Eq. (8), we expand it to the zero order, yielding a result of $(2\pi)^2$. The physical interpretation of each term in the complex expressions of Eq. (10) is summarized as follows:

- Terms depending solely on N and p represent the pure TMC contribution. In this case, this term is given by Y_A .
- Terms depending only on v_n and Ψ_n originate from collective flow. This term is given by our v_2^2 .
- Terms involving both (N, p) and (v_n, Ψ_n) arise from the interplay between TMC and flow.

Later, we will discuss three distinct contributions to the observables in both $p+p$ and $p+\text{Pb}$ collision systems, which are categorized as the ‘‘TMC terms’’, the ‘‘pure flow terms’’, and the ‘‘interplay terms.’’

Similarly, we have

$$\begin{aligned} \left\langle e^{i2(\phi_1+\phi_2-\phi_3-\phi_4)} \right\rangle_{|p_1, p_2, p_3, p_4} &= \frac{\int_0^{2\pi} e^{i2(\phi_1+\phi_2-\phi_3-\phi_4)} f_4(\vec{p}_1, \dots, \vec{p}_4) d\phi_1 d\phi_2 d\phi_3 d\phi_4}{\int_0^{2\pi} f_4(\vec{p}_1, \dots, \vec{p}_4) d\phi_1 d\phi_2 d\phi_3 d\phi_4} \\ &\approx B_0 + B_1 Y_B + \frac{1}{2} B_2 Y_B^2 + \frac{1}{6} B_3 Y_B^3 + \frac{1}{24} B_4 Y_B^4 \end{aligned} \quad (11)$$

where (assuming $p_1 = p_2 = p_3 = p_4 = p$)

$$Y_B = -\frac{p^2}{(N-4) \langle p^2 \rangle_F}, \quad (12)$$

and the full results for each order of B in Eq. (11) were presented in Ref. [70].

For $c_3\{2\}$, we have:

$$c_3\{2\} = \left\langle e^{i3(\phi_1-\phi_2)} \right\rangle, \quad (13)$$

where

$$\begin{aligned} \left\langle e^{i3(\phi_1-\phi_2)} \right\rangle_{|p_1, p_2} &= \frac{\int_0^{2\pi} e^{i3(\phi_1-\phi_2)} f_2(\vec{p}_1, \vec{p}_2) d\phi_1 d\phi_2}{\int_0^{2\pi} f_2(\vec{p}_1, \vec{p}_2) d\phi_1 d\phi_2} \\ &\approx C_0 + C_1 Y_C + \frac{1}{2} C_2 Y_C^2 + \frac{1}{6} C_3 Y_C^3. \end{aligned} \quad (14)$$

Assuming $p_1 = p_2 = p$, we obtain

$$Y_C = -\frac{p^2}{(N-2) \langle p^2 \rangle_F}, \quad (15)$$

and

$$\begin{aligned} C_0 &= v_3^2, \\ C_1 &= v_2^2 + 2v_3^2, \\ C_2 &= 4v_2^2 + 2v_2^2 v_{2F}^2 + 6v_3^2 + 3v_{2F}^2 v_3^2 - 2v_2 v_{2F} \cos(2\Psi_2), \\ C_3 &= 1 + 15v_2^2 + \frac{3v_{2F}^2}{2} + \frac{45v_2^2 v_{2F}^2}{2} + 20v_3^2 + 30v_{2F}^2 v_3^2 - 18v_2 v_{2F} \cos(2\Psi_2) - \frac{9}{2} v_2 v_{2F}^3 \cos(2\Psi_2) \\ &\quad + \frac{3}{2} v_2^2 v_{2F}^2 \cos(4\Psi_2) - \frac{1}{4} v_{2F}^3 v_3^2 \cos(6\Psi_3). \end{aligned} \quad (16)$$

In addition, for

$$c_3\{4\} = \left\langle e^{i3(\phi_1+\phi_2-\phi_3-\phi_4)} \right\rangle - 2 \left\langle e^{i3(\phi_1-\phi_2)} \right\rangle^2 \quad (17)$$

and

$$s_{C_{2,3}}\{4\} = \left\langle e^{i2(\phi_1-\phi_2)+i3(\phi_3-\phi_4)} \right\rangle - \left\langle e^{i2(\phi_1-\phi_2)} \right\rangle \left\langle e^{i3(\phi_3-\phi_4)} \right\rangle, \quad (18)$$

the specific results can be found in Refs. [70, 72].

The calculation involves several parameters, including the collective flow v_n , the transverse momentum p of the selected k -correlated particles, the mean value of p^2 over the full space $\langle p^2 \rangle_F$ and the value of v_{2F} , given by Eq. (6). In principle, N , the number of particles subject to TMC, can be regarded as another parameter. However, as seen, e.g., in Eq. (9), it always appears together with $\langle p^2 \rangle_F$. This issue will be discussed later. While these parameters are conventionally estimated using approximations from experimental data, we instead treat them as free parameters. Within a Bayesian framework, we infer the posterior distributions of these parameters directly from the experimental observables, thereby obtaining not only single-value estimates but also a complete characterization of their uncertainties. In addition, the event plane is also a parameter in the calculation results, but we find that the cumulants exhibit very weak dependence on it. Therefore, we treat it as a fixed value, where the value is taken from experimental measurements [93].

III. BAYESIAN INFERENCE

Bayesian inference provides a probabilistic framework for progressively refining estimates of model parameters. It systematically updates prior beliefs with information from observed data to yield posterior distributions, thereby quantifying the uncertainty in parameter estimation. In heavy-ion physics, Bayesian inference has found widespread application in confronting theoretical models with experimental data to extract key model parameters. The fundamental principle of Bayesian inference lies in updating our beliefs about uncertain parameters in light of empirical evidence. This process is mathematically formalized through Bayes' theorem, which defines the posterior distribution of parameters θ conditioned on the observed data D as,

$$p(\theta|D) \propto p(D|\theta)p(\theta). \quad (19)$$

In this probabilistic framework, each component plays a distinct role. The prior distribution $p(\theta)$ encapsulates our initial understanding or hypotheses about the parameters before observing the data. This can incorporate information from previous experiments, theoretical constraints, or physical boundaries, providing a rigorous means to integrate domain knowledge into the analysis. The likelihood function $p(D|\theta)$ serves as the core link between the computational model and experimental data. It quantifies the probability of observing the measured data D under the assumption that the model with parameters θ is true, effectively measuring how well different parameter configurations explain the empirical observations. The posterior distribution $p(\theta|D)$ represents the complete solution to the inverse problem, synthesizing prior knowledge with information from the observed data. This distribution provides a complete probabilistic description of parameter uncertainties, offering not only point estimates but also credible intervals and correlations between parameters.

The central objective of this work is to determine the unconstrained parameters, specifically, the genuine elliptic flow v_2 , genuine triangular flow v_3 , the transverse momentum and v_{2F} , that characterize the cumulants derived from the combined effects of TMC and collective flow. We find that the theoretical predictions exhibit only a weak dependence on v_{2F} . Consequently, while v_{2F} is included as a free parameter in the inference procedure, it does not play a central role in the subsequent analysis and will not be discussed further. In particular, as can be seen from Eqs. (9, 12, 15), the transverse momentum p^2 and $\langle p^2 \rangle_F$ only appear in the combined form of the ratio $p^2/\langle p^2 \rangle_F$. Therefore, in the Bayesian inference, we treat this ratio, denoted as $r = p^2/\langle p^2 \rangle_F$, as an independent parameter to be inferred. To achieve this, we employ experimental measurements of $c_2\{4\}$, $c_3\{2\}$, $c_3\{4\}$, and $sc_{2,3}\{4\}$ as indirect probes to infer the collective flow dynamics in small systems. These observables are chosen because they are all measured by ATLAS [90–92] under the same kinematic cuts, ensuring consistent constraints. Specifically, $c_2\{4\}$ primarily constrains v_2 , $c_3\{2\}$ and $c_3\{4\}$ constrain v_3 , and $sc_{2,3}\{4\}$ provides additional information on correlations between v_2 and v_3 , allowing for tighter constraints and more reliable inference of v_2 and v_3 in small systems. Our approach is grounded in the functional relationships $c_n\{k\} = f(v_2, v_3, r)$ provided by the TMC formalism. These expressions form the basis for constructing the likelihood function, thereby allowing a rigorous Bayesian inference of the posterior probability distributions for the parameters v_2 , v_3 , and r from the experimental data.

According to Bayes' theorem, the posterior distribution for the model parameters θ , given the experimental data y_{exp} with covariance matrix Σ_{exp} , is constructed as follows:

$$P(\theta|y_a^{\text{exp}}) = \mathcal{N}e^{-\chi^2/2}\text{Prior}(\theta) \quad (20)$$

$$\chi^2 = \sum_{a,b} (\Sigma_{\theta}^{-1})_{a,b} \Delta y_a(\theta) \Delta y_b(\theta) \quad (21)$$

where \mathcal{N} is a normalization constant, and $\Delta y_a(\theta) \equiv y_a(\theta) - y_a^{\text{exp}}$ denotes the residual between the model prediction $y_a(\theta)$ and the experimental measurement y_a^{exp} for the a -th observable. In this work, the covariance matrix Σ accounts solely for experimental uncertainties, as the theoretical predictions are computed analytically and are treated as having negligible theoretical error. For the prior $\text{Prior}(\theta)$, we adopt a uniform distribution over the possible parameter range.

To sample the posterior distribution $P(\theta|y_a^{\text{exp}})$, we employ the Markov chain Monte Carlo (MCMC) method, which generates representative samples according to the posterior distribution by making a random walk in parameter space weighted by the relative posterior probability. Denoting the parameter set in the n^{th} iteration step as $\theta^{(n)}$, MCMC samples the next step $\theta^{(n+1)}$ as a random walk starting from $\theta^{(n)}$, and decides whether to accept this update according to a probability being $p = \min[1, P(\theta^{(n+1)})/P(\theta^{(n)})]$. One can show that samples generated in such a way satisfy the desired posterior distribution $P(\theta|y_a^{\text{exp}})$. Markov chains have a property that the conditional probability distribution of future states depends only on the current state and not on the past states preceding the current one, which guarantees the stationary distribution to be achieved.

For the practical computation, we apply the Pymc framework and choose the No-U-Turn Sampler (NUTS), which is the extension to Hamiltonian Monte Carlo method [94, 95]. We take 50000 samples from each Markov chain with

iteration number of adaptive phase being 30000 to ensure decorrelation. With a sufficient amount of parameter sets (θ_i), we are able to cast them into one(two)-dimensional histograms to measure single-parameter marginal posterior distributions or two-parameter correlations.

IV. RESULTS

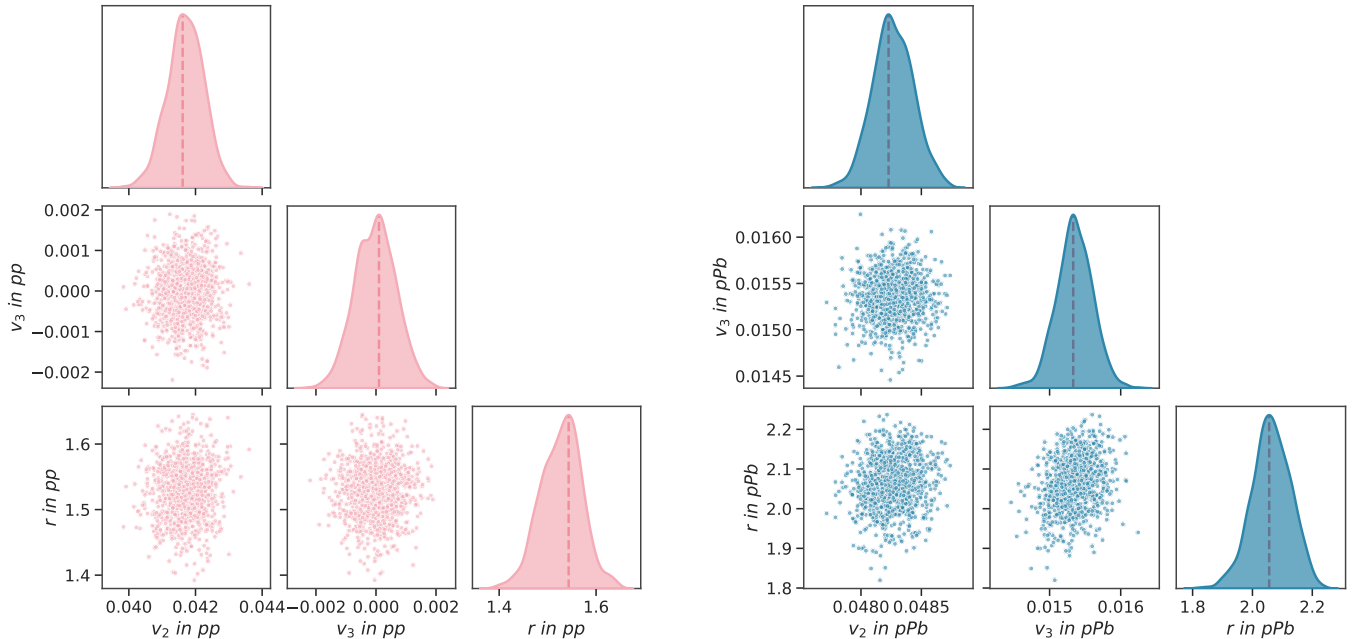


FIG. 1: Bayesian posterior probability distributions of v_2 , v_3 , and r ($r = p^2/\langle p^2 \rangle_F$) parameters from MCMC sampling. The left pairplot corresponds to $p+p$ collisions, the right to $p+Pb$ collisions. Diagonal elements represent marginal posterior distributions via kernel density estimation, and off-diagonal elements show joint posterior distributions as scatter plots, revealing inter-parameter dependencies.

This section presents the Bayesian inference results to determine the flow harmonics v_n for both $p+p$ and $p+Pb$ collision systems. The framework is built on calculations from the TMC method and constrained by key experimental observables, namely cumulants and symmetric cumulants, enabling a direct comparison of collective flow behaviors across these two distinct small collision systems. In our Bayesian analysis, we select four experimental observables which are $c_2\{4\}$, $c_3\{2\}$, $c_3\{4\}$, and $sc_{2,3}\{4\}$. The choice of these four observables is motivated by following two reasons. Firstly, from a physical perspective, they include the information about the collective flow parameters v_2 and v_3 , as well as the correlation between them; secondly, these four observables are the only available experimental data obtained under identical experimental conditions that cover both $p+p$ and $p+Pb$ collision systems [90–92]. Note that these observables depend on the charged particle multiplicity N_{ch} . In our formulas, however, N denotes the number of particles under the influence of the TMC, that is, all particles. Therefore, in the inference we assume a relation between N and N_{ch} based on isospin symmetry, $N = (3/2)N_{ch}$, so that all quantities can be expressed as functions of N_{ch} . The validity of this assumption will be discussed in Section IV B.

Our analysis proceeds in two sequential steps, with consistent methodological application to two collision systems. First, we establish a baseline for each system by treating v_2 , v_3 , and r ($r = p^2/\langle p^2 \rangle_F$) as constants, inferring their values and distributions directly from the measured cumulants $c_2\{4\}$, $c_3\{2\}$, $c_3\{4\}$, and $sc_{2,3}\{4\}$.

Second, as the charged-particle multiplicity N_{ch} increases, the particle density and the frequency of interactions in the system are expected to grow, leading to an enhancement of collective behavior. To systematically investigate the collective flow in small systems, we extend the model by introducing a functional dependence of these parameters on N_{ch} , separately for each collision system. This dependence is parameterized by a power-law form, $v_2 = a \cdot N_{ch}^b$. Here, the exponent b controls the strength of the power-law scaling and characterizes how rapidly the collective flow evolves with charged-particle multiplicity, while the prefactor a determines the overall strength of collectivity at a reference multiplicity scale. The same parameterization is applied to v_3 and r for both $p+p$ and $p+Pb$ systems. For

the exponent b , we impose a positive prior, reflecting our assumption that collectivity and transverse momentum do not decrease as N_{ch} increases.

A. Bayesian Inference of Constant Parameters

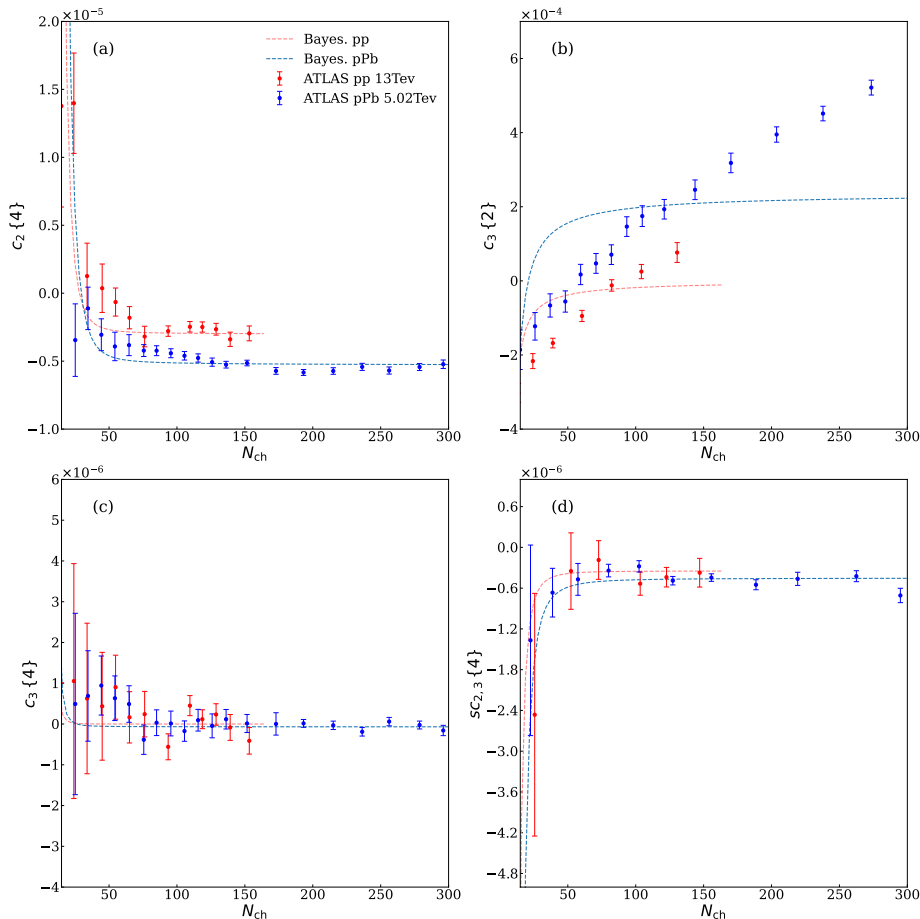


FIG. 2: Comparison between Bayesian inference results and ATLAS experimental data for cumulants and symmetric cumulants. Data points represent experimental measurements, while curves show analytical results obtained by substituting Bayesian-inferred parameters into the TMC formula. Red symbols and curves correspond to the $p+p$ system, and blue to the $p+Pb$ system.

The posterior distributions of the parameters obtained from the Markov Chain Monte Carlo (MCMC) sampling are shown in Fig. 1, which displays pairwise parameter correlations and marginalized probability densities for both $p+p$ and $p+Pb$ collision systems. For $p+p$ collisions, the maximum a posteriori (MAP) parameter values of the key baseline parameters are: $v_2^{\text{pp,MAP}} = 0.0416^{+0.0005}_{-0.0006}$, $v_3^{\text{pp,MAP}} = 0.0001^{+0.0007}_{-0.0007}$, and $r^{\text{pp,MAP}} = 1.5434^{+0.0240}_{-0.0569}$ GeV/ c ; on the other hand, the $p+Pb$ system exhibits higher maximum probability values at the baseline: $v_2^{\text{pPb,MAP}} = 0.0482^{+0.0002}_{-0.0001}$, $v_3^{\text{pPb,MAP}} = 0.0153^{+0.0003}_{-0.0002}$, and $r^{\text{pPb,MAP}} = 2.0559^{+0.0740}_{-0.0554}$ GeV/ c . These values, representing the most probable parameter estimates from the MCMC posterior, are subsequently used as core inputs for calculating the cumulants, which are then compared with experimental data.

After obtaining the posterior distributions of the inferred parameters, the cumulants are evaluated for each posterior sample. The predictions corresponding to MAP parameter values are taken as the central estimates. The associated uncertainties are quantified by the 95% credible intervals of the cumulant distributions constructed from the posterior samples. The resulting cumulants and symmetric cumulants for both $p+p$ and $p+Pb$ systems are then compared with the experimental data, as shown in Fig. 2. Depending on the maximum measured charged-particle multiplicity, our model results constrained by the experimental data are shown up to $N_{\text{ch}} = 160$ for the $p+p$ system, but up to

$N_{\text{ch}} = 300$ for the p +Pb system. The same presentation scheme is adopted in the subsequent figures for consistency. For the four-particle cumulant $c_3\{4\}$, Fig. 2 (c), and the symmetric cumulant $sc_{23}\{4\}$, Fig. 2 (d), the TMC-calculated values, with error bars reflecting the propagated uncertainties, show good agreement with the experimental data over the entire multiplicity range in both p + p and p +Pb collision systems within large experimental error bars. These results demonstrate the feasibility of extracting collective flow in small systems using the Bayesian inference approach.

However, distinct discrepancies arise for $c_2\{4\}$ in Fig. 2 (a) and $c_3\{2\}$ in Fig. 2 (b), especially for $c_3\{2\}$. The experimental data for $c_3\{2\}$ exhibits a clear upward trend, with increasing charged-particle multiplicity N_{ch} , while the calculated $c_3\{2\}$ values remain nearly constant at large N_{ch} due to the constant parameters in the baseline model. This mismatch directly demonstrates that treating v_2 , v_3 , and r as constants is insufficient to capture the real dependence of $c_2\{4\}$ and $c_3\{2\}$ observed in experiments, highlighting the need for an extended model with multiplicity-dependent parameters to capture the dependence of collectivity on N_{ch} .

B. Bayesian Inference of N_{ch} -Dependent Parameters

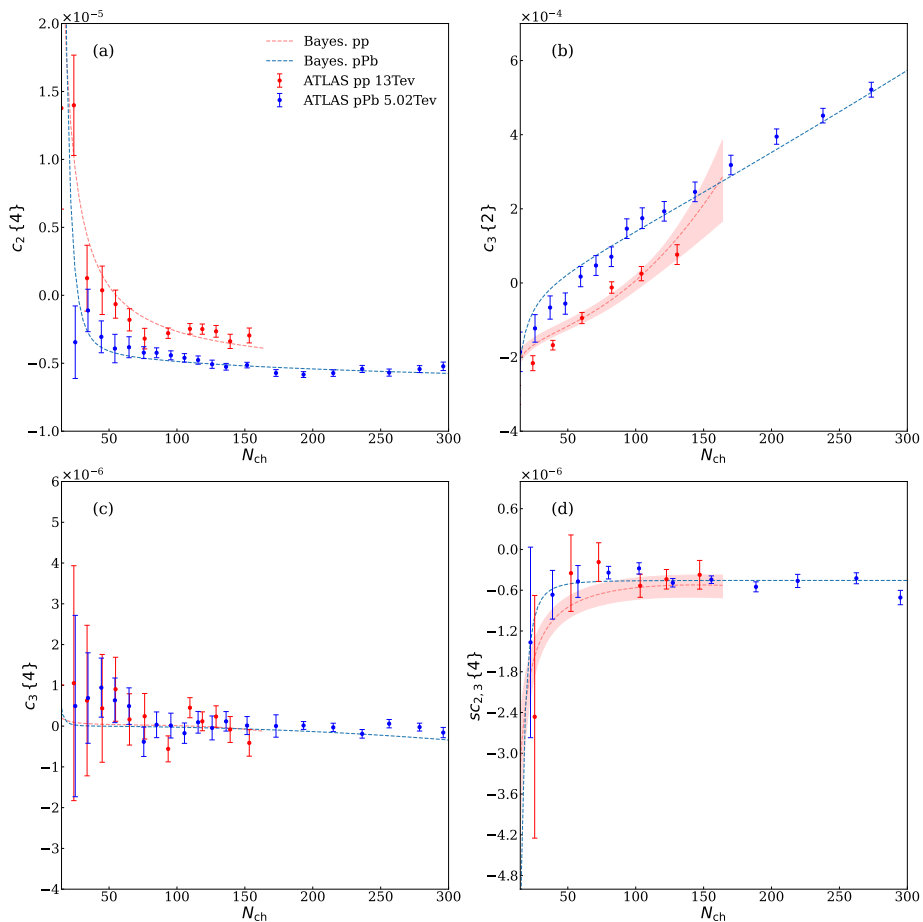


FIG. 3: Comparison of cumulants and symmetric cumulants from Bayesian inference with ATLAS experimental measurements. Symbols denote experimental measurements, and curves show TMC results using Bayesian-inferred parameters that follow a power-law scaling with N_{ch} . Red (blue) corresponds to p + p (p +Pb) collisions.

To investigate the dependence of collective flow on N_{ch} , we adopt a power-law parameterization, e.g., $v_2 = a \cdot N_{\text{ch}}^b$, which provides a simple yet flexible form to describe the observed multiplicity dependence of collective flow. After obtaining the posterior distributions of the parameters in the power-law form for v_2 , v_3 , and r , we extract the corresponding flow coefficients and transverse momentum ratio, and determine their dependence on the charged-particle multiplicity N_{ch} in small collision systems. These are subsequently incorporated into the TMC formalism, with a full propagation of the parameter uncertainties from the posterior distributions. As illustrated in Fig. 3, this

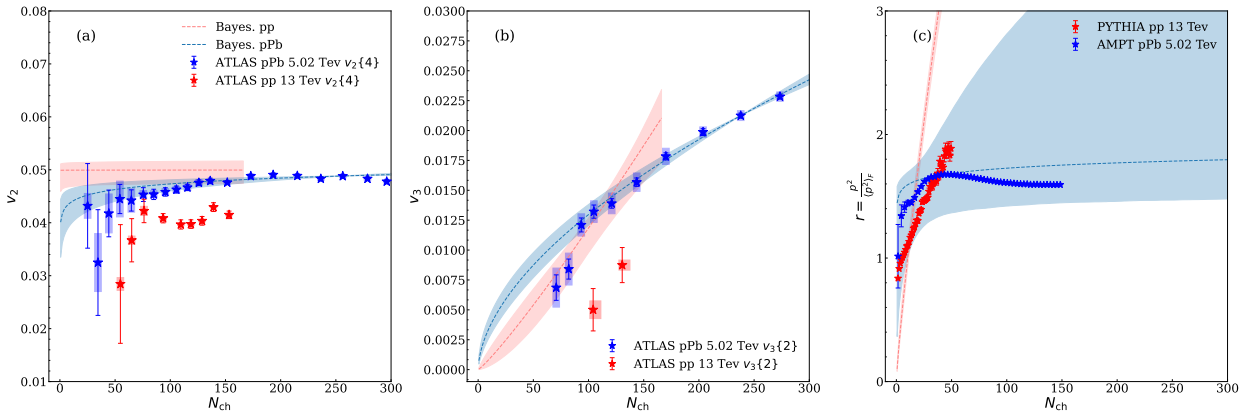


FIG. 4: Comparison of the v_2 and v_3 values extracted from cumulants with experimental data, and of the parameter r with model calculations, using PYTHIA 8 for $p+p$ and AMPT for $p+Pb$. Red and blue symbols/lines represent the $p+p$ and $p+Pb$ systems, respectively.

approach leads to an improved description of the measured cumulants, which is further confirmed by significantly smaller χ^2 values compared to the constant-parameter model discussed in the previous subsection.

Through Bayesian inference within the TMC framework constrained by experimental cumulant data, we extract the N_{ch} -dependent genuine collective flow, free from TMC contamination. In particular, Fig. 4 (a) compares our TMC-inferred results of genuine v_2 with experimental measurements of $v_2\{4\}$ in $p+p$ and $p+Pb$ collisions. We observe that the extracted genuine collective flow coefficient v_2 is generally similar between $p+p$ and $p+Pb$ collision systems. In particular, for the $p+p$ system, the inferred power-law parameter b is found to be consistent with zero, indicating that v_2 exhibits little to no dependence on N_{ch} and can be regarded as approximately constant. At low multiplicities, however, v_2 in $p+p$ appears slightly larger than in $p+Pb$, which may be attributed to stronger non-flow contributions beyond TMC in $p+p$ collisions. This overall similarity is expected, if the mechanism responsible for the generation of collective flow in small systems is the same in both cases, namely arising from event-by-event fluctuations of energy density in the initial state. In $p+Pb$ collisions, our inferred genuine collective flow v_2 is in excellent agreement with the experimental measurements of $v_2\{4\}$, which are directly obtained from $v_2\{4\} = \sqrt[4]{-c_2\{4\}}$. Note that the v_n values, along with uncertainty bands, are obtained from Bayesian analysis under the TMC framework, reflecting the genuine flow after subtracting TMC contributions. This agreement suggests that, in $p+Pb$ systems, the non-flow background contribution from TMC is effectively suppressed in the four-particle azimuthal correlations with the sub-event cumulant method.

In Fig. 4 (b), we compare our TMC-inferred results of genuine v_3 with experimental measurements of $v_3\{2\}$ in $p+p$ and $p+Pb$ collisions. Note that, in both two collision systems, the two-particle cumulant $c_3\{2\}$ becomes negative at low multiplicities, such that $v_3\{2\} = \sqrt{c_3\{2\}}$ is not defined in this region. Consequently, the experimental measurements of $v_3\{2\}$ are available only at higher multiplicities, resulting in fewer data points compared to those for $c_3\{2\}$. We observe that v_3 in $p+p$ is smaller than that in $p+Pb$ at low multiplicities, however, with increasing N_{ch} , the v_3 values between the two systems become consistent within the uncertainties. For v_3 in $p+Pb$ collisions, our results exhibit excellent agreement with experimental measurements at high N_{ch} , while at low N_{ch} they are slightly higher than the values extracted from experimental cumulants. For $p+p$ collisions, the extracted v_2 and v_3 values are systematically higher than the experimental measurements over the entire N_{ch} range. We will interpret these differences by examining the relative contributions of different components to the measured cumulants.

The extracted parameter $r = p^2 / \langle p^2 \rangle_F$ is presented in Fig. 4 (c). At low N_{ch} , the value of r in $p+Pb$ collisions is larger than that in $p+p$ collisions; As N_{ch} increases, r in $p+Pb$ collisions saturates, whereas in $p+p$ collisions it continues to increase and exceeds the $p+Pb$ values. This trend and ordering are consistent with the experimentally observed behavior of mean transverse momentum in the two systems [96]. To further validate our extraction, we compare the inferred $r = p^2 / \langle p^2 \rangle_F$ with the PYTHIA model [97] calculation in $p+p$ collisions and the AMPT model [98] calculation in $p+Pb$ collisions, where p^2 is taken as the mean squared transverse momentum in the central rapidity region and $\langle p^2 \rangle_F$ is evaluated over the full phase space. The model results reproduce the relative magnitude and trend of the extracted values of r in both $p+p$ and $p+Pb$ collision systems.

In principle, N , the number of particles subject to TMC, could be treated as an additional free parameter. However, as seen, e.g., in Eq. (9), it always appears together with r ; consequently, N and r cannot be treated as independent parameters. In our approach, we assume the relation between N and N_{ch} , $N = (3/2)N_{ch}$, and determine r . The

obtained value of r is consistent with model calculations, supporting the validity of this relation between N and N_{ch} .

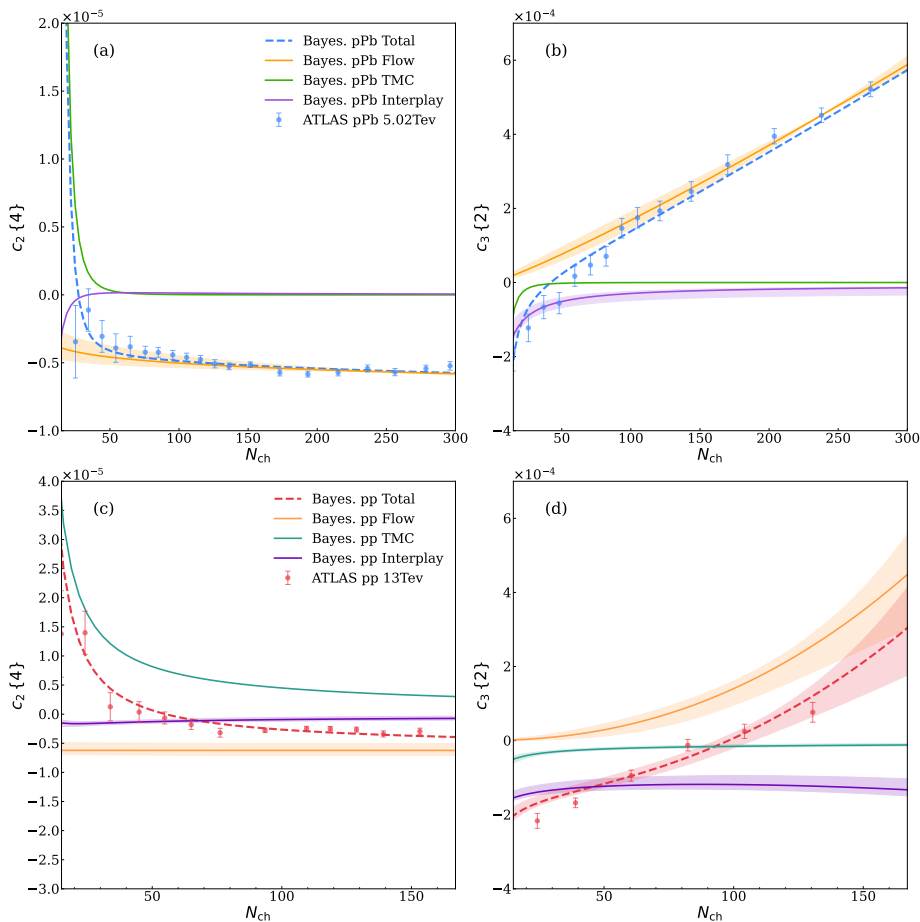


FIG. 5: Comparison between the Bayesian analytical results and experimental data for $c_2\{4\}$ and $c_3\{2\}$, decomposed into different physical contributions. The top row shows the $p+p$ system, and the bottom row the $p+Pb$ system. The yellow, green, and purple dashed lines represent the contributions from pure flow, pure TMC, and their interplay, respectively.

C. Comparative decomposition of physical contributions of Bayesian-inferred results

To understand the differences between the Bayesian-inferred v_n and the experimental measurements in $p+p$ and $p+Pb$ collisions, we decompose the theoretically calculated cumulants into three distinct contributions. This decomposition allows a clear interpretation of the experimental results, as illustrated in Fig. 5. The upper panels show $c_2\{4\}$ and $c_3\{2\}$ in $p+Pb$ collisions, while the lower two subfigures correspond to the $p+p$ system. As introduced in Section II, we analyze three distinct contributions, including the collective flow term, the TMC-only term, and the interplay term between TMC and flow, which are depicted as solid curves in yellow, green, and purple, respectively.

We first discuss the $p+Pb$ system. For $c_2\{4\}$, as shown in Fig. 5 (a), the contribution from pure collective flow alone (indicated by the yellow band) nearly reproduces all experimental data points when the multiplicity N_{ch} is larger than 50. For $c_3\{2\}$ in Fig. 5 (b), the negative values at low N_{ch} arise primarily from the interplay between TMC and collective flow, clearly indicated by the purple band. As the multiplicity increases, the contribution from pure flow grows and eventually dominates at higher N_{ch} , providing a good match with experimental data. Consequently, the extracted v_3 (Fig. 4) is slightly higher than measurements at low N_{ch} , consistent with the yellow curve lying above the data in this region. This indicates that in $p+Pb$, non-flow contributions to v_3 at low multiplicities are mainly due to TMC, which our framework quantitatively captures.

Turning to $p+p$ collisions, for $c_2\{4\}$ in Fig. 5 (c), the magnitude of the pure flow contribution (yellow band) exceeds that of negative experimental points, explaining why the extracted v_2 (Fig. 4) is systematically higher. In $p+p$

collisions, the TMC contribution cannot be neglected at any N_{ch} , as evidenced by the consistently nonzero green band. Our Bayesian approach enables the separation and subtraction of TMC-induced non-flow, allowing the extraction of the genuine collective flow v_2 . For $c_3\{2\}$ in $p+p$ collisions, as shown in Fig. 5 (d), the pure flow contribution is actually larger than the direct reflection of the experimental data, because the interplay term is significant across all N_{ch} , resulting in a negative contribution to the experimental data. It should be noted that at low N_{ch} , our result can not fully explain the experimental results, which suggests that, besides TMC, other unknown effects may also contribute to $c_3\{2\}$ in $p+p$ collisions.

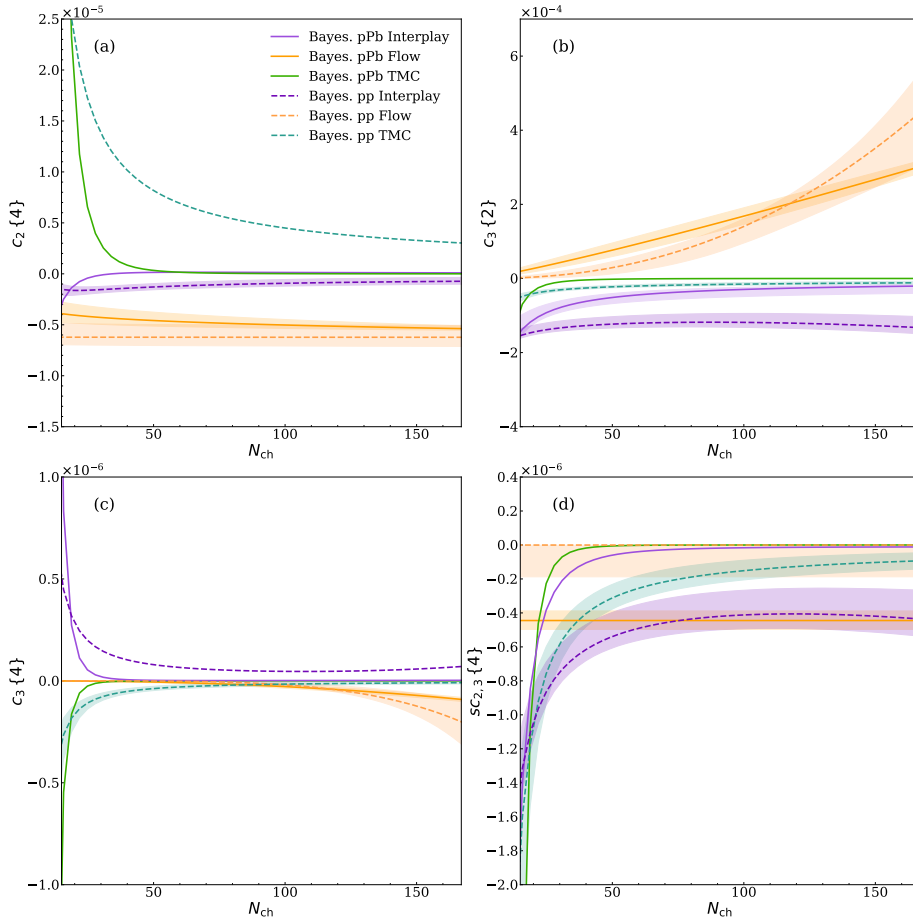


FIG. 6: Comparison of different physical contributions to $c_2\{4\}$, $c_3\{2\}$, $c_3\{4\}$ and $sc_{2,3}\{4\}$ between $p+p$ and $p+Pb$ systems. The dashed lines correspond to the $p+p$ system, and the solid lines to the $p+Pb$ system. Colors indicate the contributions: yellow for pure flow, green for pure TMC, and purple for the interplay between flow and TMC.

Finally, we perform a detailed comparison of the individual contributions to different cumulants between the two collision systems. We observe that, for $c_2\{4\}$ in Fig. 6 (a), the pure flow contribution shows no significant difference between $p+p$ and $p+Pb$ systems within uncertainties, while a stronger TMC effect is observed in the $p+p$ system than in $p+Pb$ systems. For $c_3\{2\}$ in Fig. 6 (b), a pronounced difference is observed in the interplay term between the two systems, indicating distinct correlations between flow and the TMC effect. Furthermore, in $sc_{2,3}\{4\}$ in Fig. 6 (d), the visible difference in the yellow bands clearly demonstrates a markedly different correlation between v_2 and v_3 in $p+p$ and $p+Pb$ collisions. Specifically, the v_2-v_3 correlation in $p+p$ collisions is found to be consistent with zero, whereas a significantly negative correlation is observed in the $p+Pb$ system. These observations indicate that, although the extracted v_2 and v_3 values are similar in the two small collision systems, the associated TMC effect, the interplay between TMC and flow, and the v_2-v_3 correlation differ significantly between $p+p$ and $p+Pb$ systems. The differences may be partially attributed to the distinct particle momentum distributions in the two systems, which in turn results in different TMC contributions and their interplay with collective flow. Our Bayesian analysis based on the TMC framework offers a novel tool for uncovering the physical source distinctions hidden within similar experimental data across different small collision systems.

V. CONCLUSIONS

This work employs a Bayesian inference framework, built upon the transverse momentum conservation (TMC) formalism and constrained by the experimental measurements of $c_2\{4\}$, $c_3\{2\}$, $c_3\{4\}$, and $sc_{2,3}\{4\}$, to extract the genuine collective flow behavior in $p+p$ and $p+Pb$ collisions. The analysis is conducted in two stages: first, a baseline model with constant parameters is established for each collision system; then, a refined model introduces a power-law dependence of v_2 , v_3 , and r ($r = p^2/\langle p^2 \rangle_F$) on charged-particle multiplicity. The power-law model significantly improves the description of the experimental cumulant data, yielding substantially lower χ^2 values compared to the constant-flow model.

Within the TMC theoretical framework, our approach enables a systematic disentanglement of TMC-induced nonflow effects, allowing the extraction of the genuine collective flow signal. This capability is essential for studying the nature of collectivity in small collision systems, where nonflow contributions are known to be significant. We observe that the extracted collective flow coefficients v_2 and v_3 are similar between $p+p$ and $p+Pb$ collision systems. This observation provides strong evidence that the underlying mechanism responsible for the emergence of collective flow is common to both small systems. However, the contributions from TMC, the interplay between TMC and collective flow, as well as the correlations between v_2 and v_3 , exhibit clear system-dependent differences. This demonstrates that, beyond the common origin of collective flow, more detailed and system-specific correlations differ between $p+p$ and $p+Pb$ collisions.

Moreover, this framework directly exposes the impact of TMC on flow observables and provides a quantitative assessment of true flow in small systems by isolating it from nonflow effects. In $p+Pb$ collisions, the measurement of $c_2\{4\}$ effectively suppresses nonflow effects, such that the extracted $v_2\{4\}$ is dominated by genuine collective flow. In contrast, for $c_3\{2\}$, TMC effects dominate at low charged-particle multiplicity, while at high multiplicity the observed $v_3\{2\}$ is primarily driven by true collective dynamics. In $p+p$ collisions, however, due to the fact that TMC effects remain substantial across the entire multiplicity range, the experimentally measured $v_2\{4\}$ and $v_3\{2\}$ are systematically underestimated relative to genuine v_2 and v_3 .

Overall, the combination of the TMC framework with hierarchical Bayesian inference offers a powerful approach to studying the nature of collective flow via azimuthal correlations in small collision systems. This methodology provides a unified and quantitatively controlled way to separate collective flow from nonflow contributions, thereby offering a more reliable physical interpretation of experimental data in small systems.

Acknowledgments

Shuang Guo thanks Prof. Kai Zhou for his introductory instruction in Bayesian inference framework. This work is partially supported by the National Natural Science Foundation of China under Grants No. 12325507, No. 12547102, and No. 12147101, the National Key Research and Development Program of China under Grant No. 2022YFA1604900 (S.G., J.P. and G.M.), the Ministry of Science and Higher Education (PL), and the National Science Centre (PL), Grant No. 2023/51/B/ST2/01625 (A.B.).

-
- [1] W. Busza, K. Rajagopal, and W. van der Schee, *Ann. Rev. Nucl. Part. Sci.* **68**, 339 (2018), 1802.04801.
 - [2] R. A. Lacey, N. N. Ajitanand, J. M. Alexander, P. Chung, W. G. Holzmann, M. Issah, A. Taranenko, P. Danielewicz, and H. Stoecker, *Phys. Rev. Lett.* **98**, 092301 (2007), nucl-ex/0609025.
 - [3] H.-J. Drescher, A. Dumitru, C. Gombeaud, and J.-Y. Ollitrault, *Phys. Rev. C* **76**, 024905 (2007), 0704.3553.
 - [4] J. Adams et al. (STAR), *Nucl. Phys. A* **757**, 102 (2005), nucl-ex/0501009.
 - [5] N. Brambilla et al., *Eur. Phys. J. C* **74**, 2981 (2014), 1404.3723.
 - [6] Q.-Y. Shou et al., *Nucl. Sci. Tech.* **35**, 219 (2024), 2409.17964.
 - [7] J. Chen et al., *Nucl. Sci. Tech.* **35**, 214 (2024), 2407.02935.
 - [8] U. Heinz and R. Snellings, *Ann. Rev. Nucl. Part. Sci.* **63**, 123 (2013), 1301.2826.
 - [9] H. Song and U. W. Heinz, *Phys. Rev. C* **77**, 064901 (2008), 0712.3715.
 - [10] S. Jeon and U. Heinz, *Int. J. Mod. Phys. E* **24**, 1530010 (2015), 1503.03931.
 - [11] C. Shen and L. Yan, *Nucl. Sci. Tech.* **31**, 122 (2020), 2010.12377.
 - [12] C. Gale, S. Jeon, and B. Schenke, *Int. J. Mod. Phys. A* **28**, 1340011 (2013), 1301.5893.
 - [13] L. Yan, *Chin. Phys. C* **42**, 042001 (2018), 1712.04580.
 - [14] B. Alver and G. Roland, *Phys. Rev. C* **81**, 054905 (2010), [Erratum: *Phys.Rev.C* 82, 039903 (2010)], 1003.0194.
 - [15] G.-L. Ma and X.-N. Wang, *Phys. Rev. Lett.* **106**, 162301 (2011), 1011.5249.
 - [16] L. Yan, J.-Y. Ollitrault, and A. M. Poskanzer, *Phys. Rev. C* **90**, 024903 (2014), 1405.6595.

- [17] G.-Y. Qin, H. Petersen, S. A. Bass, and B. Muller, *Phys. Rev. C* **82**, 064903 (2010), 1009.1847.
- [18] J.-Y. Ollitrault, *Phys. Rev. D* **46**, 229 (1992).
- [19] H. Stoecker, *Nucl. Phys. A* **750**, 121 (2005), nucl-th/0406018.
- [20] A. M. Poskanzer and S. A. Voloshin, *Phys. Rev. C* **58**, 1671 (1998), nucl-ex/9805001.
- [21] P. Danielewicz and G. Odyniec, *Phys. Lett. B* **157**, 146 (1985), 2109.05308.
- [22] S.-W. Lan and S.-S. Shi, *Nucl. Sci. Tech.* **33**, 21 (2022).
- [23] A. M. Poskanzer and S. A. Voloshin, *Phys. Rev. C* **58**, 1671 (1998), nucl-ex/9805001.
- [24] P. Danielewicz, *Phys. Rev. C* **51**, 716 (1995), nucl-th/9408018.
- [25] S. Chatrchyan et al. (CMS), *Phys. Rev. C* **89**, 044906 (2014), 1310.8651.
- [26] L. Ma, G. L. Ma, and Y. G. Ma, *Phys. Rev. C* **89**, 044907 (2014), 1404.5935.
- [27] J. Jia and S. Radhakrishnan, *Phys. Rev. C* **92**, 024911 (2015), 1412.4759.
- [28] C. Adler et al. (STAR), *Phys. Rev. C* **66**, 034904 (2002), nucl-ex/0206001.
- [29] B. Alver et al. (PHOBOS), *Phys. Rev. C* **81**, 034915 (2010), 1002.0534.
- [30] X.-l. Zhu, M. Bleicher, and H. Stoecker, *Phys. Rev. C* **72**, 064911 (2005), nucl-th/0509081.
- [31] N. Borghini, *Eur. Phys. J. C* **30**, 381 (2003), hep-ph/0302139.
- [32] P. Dasgupta, H.-S. Wang, and G.-L. Ma, *Phys. Rev. C* **107**, 014905 (2023), 2208.00468.
- [33] V. Khachatryan et al. (CMS), *JHEP* **09**, 091 (2010), 1009.4122.
- [34] S. Chatrchyan et al. (CMS), *Phys. Lett. B* **718**, 795 (2013), 1210.5482.
- [35] B. Abelev et al. (ALICE), *Phys. Lett. B* **719**, 29 (2013), 1212.2001.
- [36] G. Aad et al. (ATLAS), *Phys. Rev. Lett.* **110**, 182302 (2013), 1212.5198.
- [37] A. M. Sirunyan et al. (CMS), *Phys. Rev. C* **98**, 044902 (2018), 1710.07864.
- [38] S. Acharya et al. (ALICE), *Phys. Rev. Lett.* **123**, 142301 (2019), 1903.01790.
- [39] A. Adare et al. (PHENIX), *Phys. Rev. Lett.* **114**, 192301 (2015), 1404.7461.
- [40] L. Adamczyk et al. (STAR), *Phys. Lett. B* **747**, 265 (2015), 1502.07652.
- [41] C. Aidala et al. (PHENIX), *Nature Phys.* **15**, 214 (2019), 1805.02973.
- [42] U. A. Acharya et al. (PHENIX), *Phys. Rev. C* **105**, 024901 (2022), 2107.06634.
- [43] N. J. Abdulameer et al. (PHENIX), *Phys. Rev. C* **107**, 024907 (2023), 2203.09894.
- [44] B. I. Abelev et al. (STAR), *Phys. Rev. C* **80**, 064912 (2009), 0909.0191.
- [45] G. Aad et al. (ATLAS), *Phys. Rev. C* **86**, 014907 (2012), 1203.3087.
- [46] P. Bozek, *Phys. Rev. C* **85**, 014911 (2012), 1112.0915.
- [47] P. Bozek, A. Bzdak, and G.-L. Ma, *Phys. Lett. B* **748**, 301 (2015), 1503.03655.
- [48] E. Shuryak and I. Zahed, *Phys. Rev. C* **88**, 044915 (2013), 1301.4470.
- [49] A. Bzdak, B. Schenke, P. Tribedy, and R. Venugopalan, *Phys. Rev. C* **87**, 064906 (2013), 1304.3403.
- [50] G.-Y. Qin and B. Müller, *Phys. Rev. C* **89**, 044902 (2014), 1306.3439.
- [51] A. Bzdak and G.-L. Ma, *Phys. Rev. Lett.* **113**, 252301 (2014), 1406.2804.
- [52] L. He, T. Edmonds, Z.-W. Lin, F. Liu, D. Molnar, and F. Wang, *Phys. Lett. B* **753**, 506 (2016), 1502.05572.
- [53] Z.-W. Lin, L. He, T. Edmonds, F. Liu, D. Molnar, and F. Wang, *Nucl. Phys. A* **956**, 316 (2016), 1512.06465.
- [54] G.-L. Ma and A. Bzdak, *Nucl. Phys. A* **956**, 745 (2016).
- [55] S.-Y. Tang, L. Zheng, X.-M. Zhang, and R.-Z. Wan, *Nucl. Sci. Tech.* **35**, 32 (2024), 2303.06577.
- [56] E. Alhassan, D. Roehman, G. Schnabel, and A. J. Koning, *Nucl. Sci. Tech.* **35**, 205 (2024), 2402.14363.
- [57] A. Dumitru, K. Dusling, F. Gelis, J. Jalilian-Marian, T. Lappi, and R. Venugopalan, *Phys. Lett. B* **697**, 21 (2011), 1009.5295.
- [58] M. Nie, L. Yi, G. Ma, and J. Jia, *Phys. Rev. C* **100**, 064905 (2019), 1906.01422.
- [59] H. Mäntysaari, *Rept. Prog. Phys.* **83**, 082201 (2020), 2001.10705.
- [60] K. Dusling and R. Venugopalan, *Phys. Rev. D* **87**, 094034 (2013), 1302.7018.
- [61] B. Schenke, *Rept. Prog. Phys.* **84**, 082301 (2021), 2102.11189.
- [62] M. Mace, V. V. Skokov, P. Tribedy, and R. Venugopalan, *Phys. Rev. Lett.* **121**, 052301 (2018), [Erratum: *Phys.Rev.Lett.* **123**, 039901 (2019)], 1805.09342.
- [63] H. Mäntysaari and B. Schenke, *Phys. Rev. Lett.* **117**, 052301 (2016), 1603.04349.
- [64] Z. Chajeccki and M. Lisa, *Phys. Rev. C* **78**, 064903 (2008), 0803.0022.
- [65] Z. Chajeccki and M. Lisa, *Phys. Rev. C* **79**, 034908 (2009), 0807.3569.
- [66] S. Pratt, S. Schlichting, and S. Gavin, *Phys. Rev. C* **84**, 024909 (2011), 1011.6053.
- [67] A. Bzdak, V. Koch, and J. Liao, *Phys. Rev. C* **83**, 014905 (2011), 1008.4919.
- [68] A. Bzdak and G.-L. Ma, *Phys. Rev. C* **97**, 014903 (2018), 1710.00653.
- [69] A. Bzdak and G.-L. Ma, *Phys. Lett. B* **781**, 117 (2018), 1801.01277.
- [70] M.-T. Xie, G.-L. Ma, and A. Bzdak, *Phys. Rev. C* **105**, 054904 (2022), 2204.01038.
- [71] J.-L. Pei, G.-L. Ma, and A. Bzdak, *Phys. Rev. C* **110**, 024901 (2024), 2403.05782.
- [72] J.-L. Pei, G.-L. Ma, and A. Bzdak, *Phys. Rev. C* **112**, 034909 (2025), 2503.12846.
- [73] J. E. Bernhard, Ph.D. thesis, Duke U. (2018), 1804.06469.
- [74] J. E. Bernhard, J. S. Moreland, S. A. Bass, J. Liu, and U. Heinz, *Phys. Rev. C* **94**, 024907 (2016), 1605.03954.
- [75] J. E. Bernhard, J. S. Moreland, and S. A. Bass, *Nature Phys.* **15**, 1113 (2019).
- [76] D. Everett et al. (JETSCAPE), *Phys. Rev. Lett.* **126**, 242301 (2021), 2010.03928.
- [77] D. Everett et al. (JETSCAPE), *Phys. Rev. C* **103**, 054904 (2021), 2011.01430.
- [78] S. Cao et al. (JETSCAPE), *Phys. Rev. C* **104**, 024905 (2021), 2102.11337.

- [79] G. Nijs, W. van der Schee, U. Gürsoy, and R. Snellings, *Phys. Rev. C* **103**, 054909 (2021), 2010.15134.
- [80] G. Nijs, W. van der Schee, U. Gürsoy, and R. Snellings, *Phys. Rev. Lett.* **126**, 202301 (2021), 2010.15130.
- [81] J. E. Parkkila, A. Onnerstad, and D. J. Kim, *Phys. Rev. C* **104**, 054904 (2021), 2106.05019.
- [82] G. Giacalone, G. Nijs, and W. van der Schee, *Phys. Rev. Lett.* **131**, 202302 (2023), 2305.00015.
- [83] Y.-L. Cheng, S. Shi, Y.-G. Ma, H. Stöcker, and K. Zhou, *Phys. Rev. C* **107**, 064909 (2023), 2301.03910.
- [84] S. Pratt, E. Sangaline, P. Sorensen, and H. Wang, *Phys. Rev. Lett.* **114**, 202301 (2015), 1501.04042.
- [85] M. Omana Kuttan, J. Steinheimer, K. Zhou, and H. Stoecker, *Phys. Rev. Lett.* **131**, 202303 (2023), 2211.11670.
- [86] J. M. Wang, X. G. Deng, W. J. Xie, B. A. Li, and Y. G. Ma, *Chin. Phys.* **49**, 124105 (2025), 2406.07051.
- [87] G. Wei, M. Nan, P. Li, Y. Wang, Q. Li, G. Yong, and F. Liu, *Phys. Rev. C* **113**, 024910 (2026), 2509.03406.
- [88] L.-Q. Zhu, O.-Y. Luo, X. Chen, K. Zhou, H.-Z. Zhang, and D.-F. Hou, *Nucl. Sci. Tech.* **37**, 68 (2026), 2508.12756.
- [89] Y. He, L.-G. Pang, and X.-N. Wang, *Phys. Rev. Lett.* **122**, 252302 (2019), 1808.05310.
- [90] M. Aaboud et al. (ATLAS), *Phys. Lett. B* **789**, 444 (2019), 1807.02012.
- [91] M. Aaboud et al. (ATLAS), *Phys. Rev. C* **97**, 024904 (2018), 1708.03559.
- [92] M. Aaboud et al. (ATLAS), *Eur. Phys. J. C* **77**, 428 (2017), 1705.04176.
- [93] S. Acharya et al. (ALICE), *Eur. Phys. J. C* **83**, 576 (2023), 2302.01234.
- [94] J. Salvatier, T. V. Wiecki, and C. Fonnesbeck, *PeerJ Comput. Sci.* **2**, e55 (2016), 1507.08050.
- [95] M. D. Hoffman and A. Gelman, *J. Mach. Learn. Res.* **15**, 1593 (2014), 1111.4246.
- [96] B. B. Abelev et al. (ALICE), *Phys. Lett. B* **727**, 371 (2013), 1307.1094.
- [97] T. Sjostrand, S. Mrenna, and P. Z. Skands, *Comput. Phys. Commun.* **178**, 852 (2008), 0710.3820.
- [98] Z.-W. Lin, C. M. Ko, B.-A. Li, B. Zhang, and S. Pal, *Phys. Rev. C* **72**, 064901 (2005), nucl-th/0411110.